# Improving timing performance of double-ended readout in TOF-PET detectors

**L. Guo,**[a,b,c,d] **J. Tian,**[b,d] **P. Chen,**[b,d] **S.E. Derenzo**[a] **and W.-S. Choong**[a,1]

[a]*Molecular Biophysics and Integrated Bioimaging Division, Lawrence Berkeley National Laboratory,*
*1 Cyclotron Road, Berkeley, CA 94720, U.S.A.*

[b]*Key Laboratory of Ultra-fast photoelectric Diagnostics Technology,*
*Xi'an Institute of Optics and Precision Mechanics, Chinese Academy of Sciences,*
*No. 17 Xinxi Road, Xi'an 710119, China*

[c]*College of Materials Science and Opto-Electronic Technology, University of Chinese Academy of Sciences,*
*No. 19 Yuquan Road, Beijing 100049, China*

[d]*Collaborative Innovation Center of Extreme Optics, Shanxi University,*
*No. 92 Wucheng Road, Taiyuan 030006, China*

*E-mail:* wschoong@lbl.gov

ABSTRACT: Scintillation crystals of 20 mm length or longer are needed for clinical time-of-flight positron emission tomography (TOF-PET) to ensure effective detection efficiency for gamma photons. However, the use of long crystals would deteriorate the key performance of TOF-PET detectors, time and spatial resolution, because of the variations in the travel times of the photons in crystals and the effects of parallax errors. In this work, we studied double-ended readout TOF-PET detectors based on coupling a long scintillation crystal to SiPMs at both ends for correcting the depth-dependent effects to improve the coincidence time resolution (CTR). In particular, we focused our attention to analyze timing performance using different correction methods, including trigger times of the individual photodetectors at both ends of the crystal, the simple average of the trigger times, and the weighted average based on the inverse variances of the depth-dependent corrected trigger times. For a 3 mm × 3 mm × 25 mm unpolished lutetium fine silicate (LFS) crystal with double-ended readout and practical head-on irradiation, a CTR of 246 ps FWHM can be achieved using depth-dependent timing-correction and weighted average time method compared to 280 ps FWHM using the conventional simple average time method and 393 ps FWHM using the conventional single-ended readout. The results show that the depth-dependent timing-correction and weighted average time method in double-ended readout can effectively correct for the trigger time variations in TOF-PET detector utilizing long unpolished crystals, resulting in an improvement in the CTR of as much as 37% compared to single-ended readout.

KEYWORDS: Gamma camera, SPECT, PET PET/CT, coronary CT angiography (CTA); Instrumentation for gamma-electron therapy

---

[1]Corresponding author.

# Contents

# 1 Introduction

TOF-PET scanner [1, 2] is a complex three-dimensional imaging system and has become an important medical apparatus for monitoring cell activity and metabolic processes of organisms. Compared to the conventional non-TOF PET scanner, it can improve reconstructed image signal-to-noise ratio (SNR) by providing localizations of the positron emission points using the TOF information. In modern whole-body PET systems, better time resolution and higher sensitivity are the keys to improve the SNR while reducing patient injection radiation dose and exposure times. Research has shown that time resolution will improve as crystal length decreases [3]. While excellent CTRs of sub-100 ps FWHM have been achieved using 3–5 mm short and fast crystals, such as L(Y)SO:Ce:Ca and LaBr3:Ce [4]–[7], the crystals are too short to stop more gamma photons effectively. To detect the radiation effectively, the length of the crystals used in clinical TOF-PET scanners is usually 20 mm or longer which in turn causes deterioration in the time resolution and parallax errors due to DOI uncertainty. With the aid of the fast waveform digitizers, deep convolutional neural networks were applied innovatively to estimate TOF directly and CTR has been improved up to 23% for detectors with $5 \times 5 \times 10$ mm LFS crystals [8]. To reduce parallax errors, several methods for DOI determination of annihilation photons in TOF-PET detectors based on monolithic scintillators have been proposed [9, 10]. The concept of TOF-PET detector with double-ended readout was also proposed for improving the time and spatial resolution [11, 12]. Satisfactory DOI resolution has been demonstrated using unpolished crystals with double-ended readout [13, 14]. In addition, the timing performance for 20 mm and 30 mm length crystals with side excitation along the crystal length has been shown to improve in double-ended readout detectors

using a simple averaging of the trigger times of two photodetectors [15, 16]. However, the depth-dependent variations of annihilation photons travel times, the variations of optical photons travel times within long crystals and different pulse heights between two photodetectors at the ends of the crystal are not considered in previous experimental studies. We have shown that the contributions to the time resolution from these physical factors can be non-negligible in our previous Monte Carlo calculations [17]. The simulation results show the opportunities for improving timing performance of TOF-PET detectors with double-ended readout by correcting the depth-dependent arrival times of the photons and pulse heights [17].

The goal of our study is not so much to achieve the best timing resolution, but to study the timing performance of double-ended readout detectors compared to conventional readout methods. In this work, we evaluated the performance of scintillator detectors based on 3 mm × 3 mm × 25 mm LFS crystals with both conventional single-ended readout and double-ended readout irradiated from a practical head-on direction to validate our previous simulation studies. The flood histogram and timing resolution performance were investigated respectively. Timing performance with double-ended readout were compared using different correction methods to investigate the effects of the annihilation and optical photons travel times and pulse height within the crystal.

## 2 Materials and methods

### 2.1 Experimental setups

The experimental setup to measure the CTR of single-ended readout detectors is shown in figure 1a. A 0.5 mm Ge-68 point source was placed between two LFS crystals coupled with 3 mm × 3 mm S12572-050P MPPC SiPMs manufactured by Hamamatsu using optical grease. The sides of the crystals that were not coupled to the SiPMs were wrapped with more than 3 layers of Teflon tape to ensure negligible light leaks. The SiPMs outputs were terminated with 50 ohm resistors. The analog waveforms were digitized using the Domino Ring Sampler (DRS) evaluation board from the Paul Scherrer Institut (PSI) [18]. The DRS4 chip is based on switched capacitor array (SCA) technology. Some of its features include low power consumption, high channel density, good signal-to-noise ratio, fast sampling rate, and large cell depth to sample the complete waveform from conventional and advanced PET detectors. The DRS4 input also has a high-input analog bandwidth of 700 MHz. The analog waveforms were digitized in 1024 samples at 5 GSPS and saved in binary formats for offline processing. Because of the input range of ±500 mV in DRS4 chip, high-bandwith attenuators were applied to the outputs of SiPMs to adjust the pulse heights to meet the input dynamic range of the DRS4 chip. Energy and timing information were obtained simultaneously from the pulse. Detectors with LFS crystals of different lengths as the test scintillator detectors were investigated as shown in figure 1a. A 3 mm × 3 mm × 3 mm LFS crystal coupled to a SiPM was used as a reference scintillator detector in the CTR measurements.

We calibrated the DOI information using a 3 mm × 3 mm × 25 mm unpolished LFS crystal irradiated from the side uniformly in singles mode, as shown in figure 1b. The side surfaces of the unpolished LFS crystal were finished with 1000 grit sand papers. The total deposited energy in the crystal was calculated by summing the energies measured by the two photodetectors coupled at the ends of the crystal. Thus when the crystal is irradiated from a practical head-on direction, we can deduce DOI via calculating an energy ratio.

Figure 1c shows the schematic diagram and photo of the experimental setup for double-ended readout with head-on irradiation. The 3 mm × 3 mm × 25 mm polished and unpolished LFS crystals with double-ended readout as the test detector were measured respectively. They were in coincidence with a 3 mm × 3 mm × 3 mm LFS crystal employing single-ended readout as a reference detector.

Figure 2 shows the crystals we used. All experimental setups were operated at room temperature using the same read-out system in a light tight box. 50000 coincidence events were collected in each measurement.
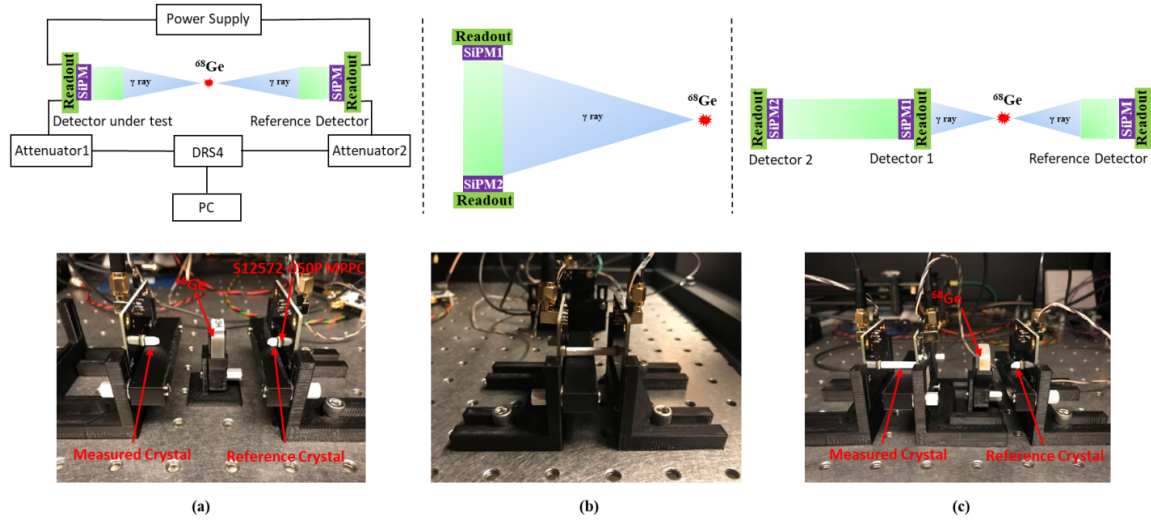


**Figure 1**. (Top) Schematic diagrams and (bottom) photos of the experimental setups for (a) coincidence time resolution measurements with conventional single-ended readout. (b) DOI calibration with side irradiation uniformly in singles mode. (c) Double-ended readout with head-on irradiation against the reference scintillator detector, respectively.
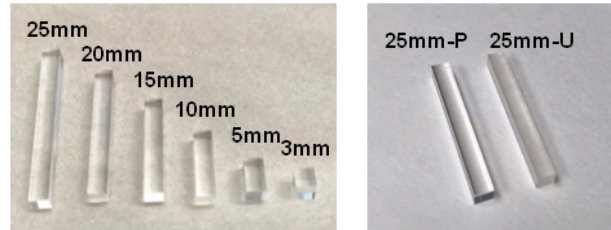


**Figure 2**. (Left) Polished LFS crystals of different lengths with 3 mm × 3 mm cross section. (Right) 3 mm × 3 mm × 25 mm polished and unpolished LFS crystals.

## 2.2 Data analysis

To reduce the effect of pile-up on the signal pulses due to dark noise, a baseline-shift method was utilized to correct the raw signal pulses. Trigger times were obtained by leading-edge time pickoff method using constant trigger thresholds. CTR value was then determined from the time difference spectrum of the coincidence events between two scintillators. The trigger threshold was swept

to determine the optimal CTR FWHM. The energy information was calculated by integrating the area under the pulse. The CTR for a pair of the same test scintillator detectors was calculated by subtracting the timing resolution of the reference detector from the measured CTR and multiplying by the square root of two:

$$\text{CTR}_\text{cal} = \sqrt{2} \cdot \sqrt{\text{CTR}_\text{mea}^2 - \frac{\text{CTR}_\text{ref}^2}{2}} \tag{2.1}$$

where $\text{CTR}_\text{mea}$ is the measured coincidence time resolution of the scintillator detector under test in coincidence with the reference scintillator detector, $\text{CTR}_\text{ref}$ is the coincidence time resolution measured with two reference detectors.

The DOI ratio was estimated using the following equation:

$$\text{DOI ratio} = \frac{E_1}{E_1 + E_2} \tag{2.2}$$

where $E_1$ and $E_2$ are the energies measured by photodetectors 1 and 2, respectively. Previous studies have shown that the DOI ratio calculated from equation (2.2) is approximately linear with the depth of interaction [19, 20]. As a result, we did not perform a point-by-point calibration of the long crystal. We irradiated the crystal from the side uniformly to calibrate the DOI ratio as discussed in section 3.2.

For double-ended readout, different correction methods were utilized to determine the influence of time variations resulting from the travel times of the annihilation photons, time delays, and dispersion of the optical photons in the crystal on the CTR [17]. Figure 3 shows a diagram of an annihilation photon interacting at a depth Z in the crystal and the optical photons detected by photodetectors 1 and 2, respectively. The time dispersions of the optical photons and light outputs at both ends of the crystal could be different because of the different propagation lengths of the optical photons to the photodetectors 1 and 2. This may result in different variations in the trigger times of the photodetectors. We employed four different methods to estimate the CTR in the double-ended readout.
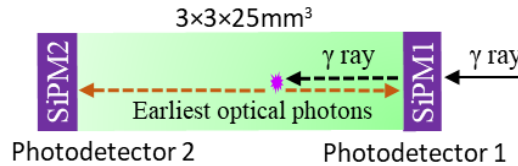


**Figure 3**. The diagram of an annihilation photon interacts at depth Z and the optical photons detected by photodetectors 1 and 2, respectively.

For method 1, we calculated the trigger time of the test detector by taking a simple average of the trigger times of the photodetectors 1 and 2, which is a common method of combining the trigger times from the two photodetectors in a double-ended readout detector [15, 16]. The simple average corrects for the optical photon transit time, but not the depth-dependent annihilation photon transit time or any trigger delay [17]. A simple average is calculated as the trigger time of the test detector:

$$T_S = \frac{T_\text{SiPM1} + T_\text{SiPM2}}{2} \tag{2.3}$$

where $T_\text{SiPM1}$ and $T_\text{SiPM2}$ are the trigger times from photodetectors 1 and 2, respectively.

For method 2, we estimated the entrance times of the annihilation photon into front surface of the crystal by correcting for the depth-dependent annihilation photon transit time. The depth Z of the annihilation photon is acquired using the DOI calibration information. The entrance times of the annihilation photon can be estimated separately as:

$$E_{\text{SiPM1}} = T_{\text{SiPM1}} - \frac{Z}{c} - \frac{nZ}{c} \tag{2.4}$$

$$E_{\text{SiPM2}} = T_{\text{SiPM2}} - \frac{Z}{c} - \frac{n(L - Z)}{c} \tag{2.5}$$

where $Z$ is the interaction depth obtained from DOI calibration information, $c$ is speed of light, $n = 1.8$ is refractive index of the LFS crystal, $L$ is the length of the LFS crystal. A simple average is then calculated as the trigger time of the test detector:

$$T_{\text{SE}} = \frac{E_{\text{SiPM1}} + E_{\text{SiPM2}}}{2} \tag{2.6}$$

For method 3, we correct for any residual time dependence variations on the DOI, which may include variation in the trigger delay from the arrival of the direct optical photons at the photodetector [17], by looking at the correlation between the entrance times and the DOI ratio. The entrance times are then corrected to offset any observed correlation. A simple average is then calculated as the trigger time of the test detector:

$$T_{\text{SEC}} = \frac{E_{\text{SiPM1}} - t_{\text{rel}E1} + E_{\text{SiPM2}} - t_{\text{rel}E2}}{2} \tag{2.7}$$

where $t_{\text{rel}E1}$ and $t_{\text{rel}E2}$ are the depth-dependent correction factors obtained from the correlation between the entrance times and the DOI ratio. In general, the trigger times of photodetectors 1 and 2 have different variances because one photodetector receives a larger fraction of the optical photons and less optical photon time dispersion than the other. Thus, a simple average is not the best statistical estimator of the trigger time. A better method is to weight the corrected trigger times estimated from each photodetector by the inverse of their variances [17]. The weighted average is calculated as:

$$T_{\text{WEC}} = W_{E1} \times (E_{\text{SiPM1}} - t_{\text{rel}E1}) + W_{E2} \times (E_{\text{SiPM2}} - t_{\text{rel}E2}) \tag{2.8}$$

where $W_{E1}$ and $W_{E2}$ are the inverse variance weighting factors of the corresponding corrected entrance times. $W_{E1}$ and $W_{E2}$ are functions of the DOI ratio and are normalized such that $W_{E1} + W_{E2} = 1$.

For method 4, we correct for any depth-dependent variations on the trigger times of photodetectors 1 and 2 by looking at the correlation between the photodetector trigger times and the DOI ratio. This effectively would include the correlation from the depth-dependent annihilation photon transit time as estimated using the entrance of the annihilation photon in method 3. The photodetector trigger times are then corrected to offset any observed correlation. Similarly, the simple and weighted averages are calculated as the trigger time of the test detector:

$$T_{\text{SC}} = \frac{T_{\text{SiPM1}} - t_{\text{rel}1} + T_{\text{SiPM2}} - t_{\text{rel}2}}{2} \tag{2.9}$$

$$T_{\text{WC}} = W_{T1} \times (T_{\text{SiPM1}} - t_{\text{rel}1}) + W_{T2} \times (T_{\text{SiPM2}} - t_{\text{rel}2}) \tag{2.10}$$

where $t_{\rm rel1}$ and $t_{\rm rel2}$ are the depth-dependent correction factors obtained from the correlation between the photodetector trigger times and the DOI ratio, and $W_{T1}$ and $W_{T2}$ are the normalized inverse variance weighting factors of the corresponding corrected photodetector trigger times.

# 3 Results and discussion

## 3.1 Single-ended readout

Figure 4 depicts the CTR FWHM of a pair of reference detectors based on 3 mm × 3 mm × 3 mm polished LFS crystals as a function of bias voltage at optimal trigger threshold. We compared the CTR performance determined by raw pulses and pulses using baseline-shift method. The baseline can be corrected by averaging parts of the signal before the risetime of the pulse and shifting the baseline to zero. We observed that the CTR decreases to an optimum value and then increases with increasing bias voltage. After applying the baseline correction, the CTR improves. This may suggest that timing jitter due to the piled-up dark noise from the SiPM is degrading the CTR. As the bias voltage increases, the dark count noise of the SiPMs gradually become the dominant noise compared to the electronics noise leading degraded CTR. For the reference detector with 3 mm × 3 mm × 3 mm polished crystal, the best CTR of 188 ps was found at 68.5 V bias-voltage. Since all the SIPMs were procured from the same batch and have similar breakdown voltages, we applied the optimal bias-voltage of 68.5 V for all SiPMs and processed the raw pulses with baseline correction in the follow-up experiments.
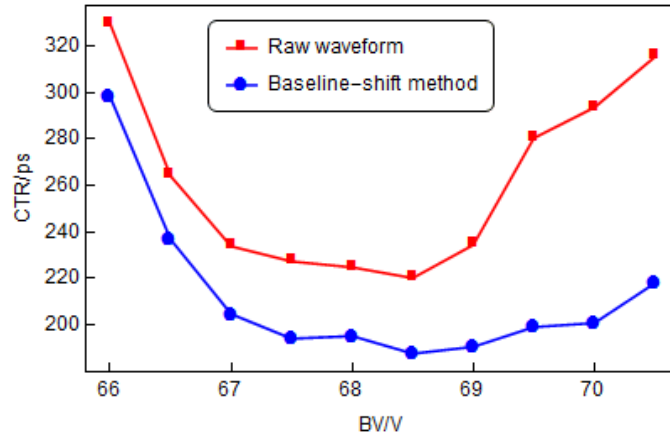


**Figure 4**. CTR of the reference scintillator detector as a function of bias voltage.

Figure 5 shows the influence of the polished crystal length on the measured CTR against the reference detector at the bias voltage of 68.5 V and optimal trigger threshold. As expected, the timing performance of test detector deteriorates as crystal length increases. It indicates that the impact of photon interaction point in long crystals on CTR will be non-negligible. The measured CTRs and corresponding calculated CTRs for pairs of the same detectors using equation (2.1) are summarized in table 1.

The measured CTRs of 25 mm long crystals with polished and unpolished surfaces were compared in figure 6. The corresponding calculated CTR for pairs of the same measured scintillator detectors were 274 ps and 393 ps respectively by equation (2.1). It indicates surface treatment of the scintillator crystal has a huge impact on the timing performance of detector.
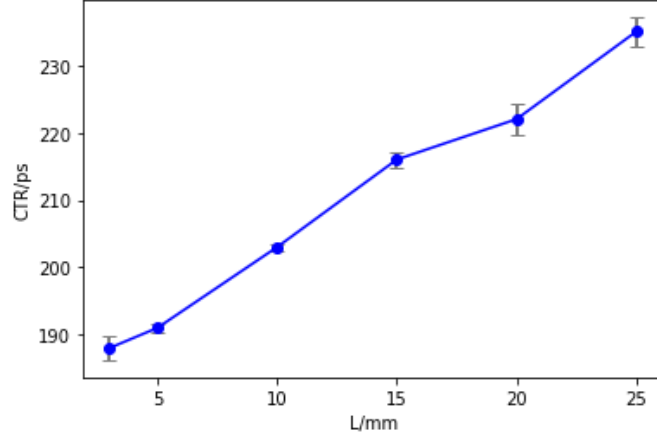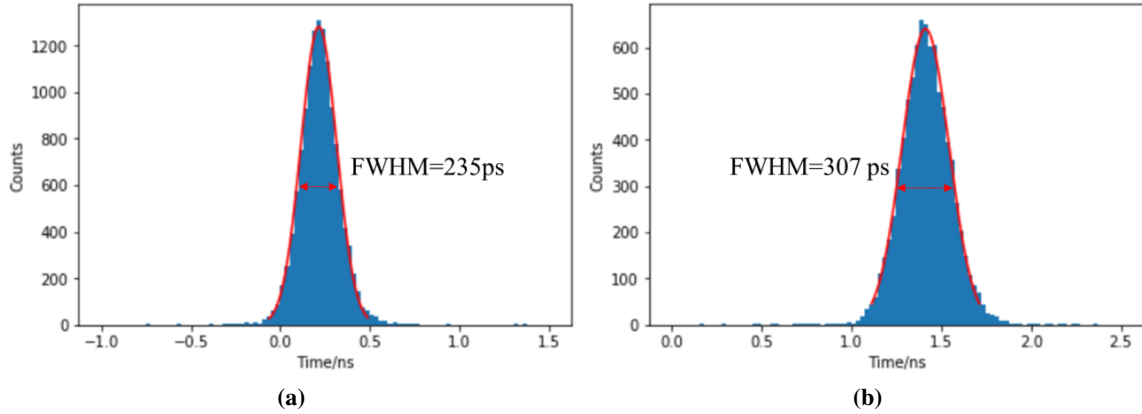
**Figure 5**. Measured single-ended readout CTR as a function of crystal length for polished crystals.

**Table 1**. Measured single-ended readout CTRs and corresponding calculated CTRs for pairs of test detectors.

| Length | Measured CTR | Calculated CTR |
|--------|--------------|----------------|
| 3 mm | 188 ps | 188 ps |
| 5 mm | 191 ps | 195 ps |
| 10 mm | 203 ps | 216 ps |
| 15 mm | 216 ps | 241 ps |
| 20 mm | 222 ps | 251 ps |
| 25 mm | 235 ps | 274 ps |



**Figure 6**. Measured single-ended readout CTRs of scintillator detector based on 3 mm × 3 mm × 25 mm LFS crystal with (a) polished surfaces and (b) unpolished surfaces, respectively.

## 3.2 DOI calibration

Figure 7 shows the normalized DOI responses of 3 mm × 3 mm × 25 mm crystals with polished and unpolished surfaces, respectively during side irradiation (SI). For double-ended readout, the optical

photons are shared between the two SiPMs coupled at the ends of the crystal. In order to have good DOI capability, we expect to have a wide uniform distribution in figure 7. The result shows that unpolished crystals provide significantly better DOI capability than polished crystals. The optical reflection in polished crystal is specular, resulting in light transmission that is independent on the DOI. On the other hand, the optical reflection in unpolished crystal is more diffuse, resulting in different light transmission detected at both end of the crystal that is dependent on the DOI. During head-on irradiation (HI), the DOI ratio is exponentially distributed along the length of the 25 mm unpolished crystal as would be expected from the exponential decay probability of the annihilation photon interaction in the crystal. We assume that the DOI ratio as calculated in equation (2.2) follows a linear relationship with the interaction depth of the annihilation photon, which is supported by other measurements [19, 20]. Since the signal decreases with increasing distance to the interaction point, we took the DOI ratio at half of the maximum counts at the left and right edges of the distribution to correspond to the interaction depths of 25 and 0 mm respectively as shown in figure 8. With this calibration, the DOI ratio is used to determine the annihilation photon interaction depth.
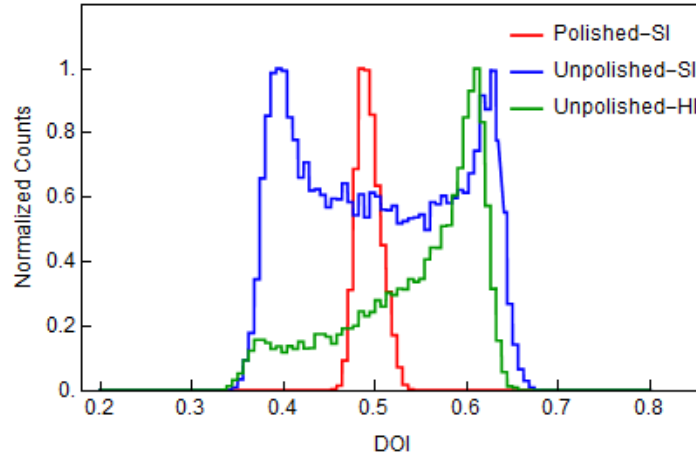


**Figure 7**. Normalized DOI responses of 3 mm × 3 mm × 25 mm LFS crystals. SI and HI represent side and head-on irradiation, respectively.
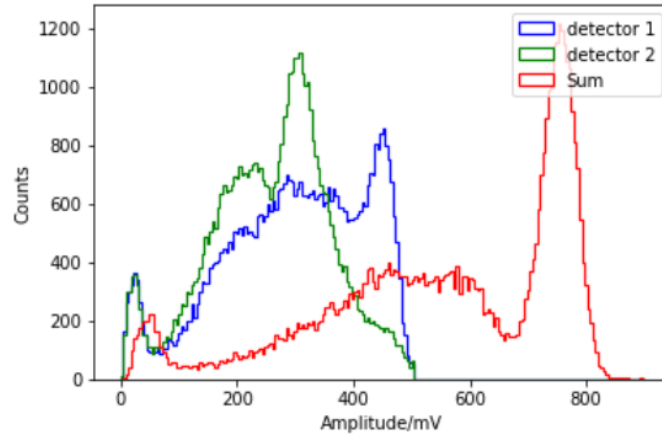
### 3.3  Double-ended readout

The energy spectrum of the scintillator detector with double-ended readout employing a 3 mm × 3 mm × 25 mm unpolished crystal is shown in figure 9. It illustrates that most of the pulse heights from the individual photodetector 1 are higher than those from the photodetector 2, which indicates that a larger number of photons are detected by photodetector 1 than photodetector 2 on average. An energy resolution of 9.1% is obtained by summing the two energies from photodetector 1 and 2.

The CTR of the test detector with double-ended readout was measured against the reference detector. To investigate the effect of depth-dependent travel times of annihilation and optical photons within the crystal and light outputs between two photodetectors at ends of the crystal on timing performance, we compared the CTR values using equation (2.3)–(2.10) respectively.
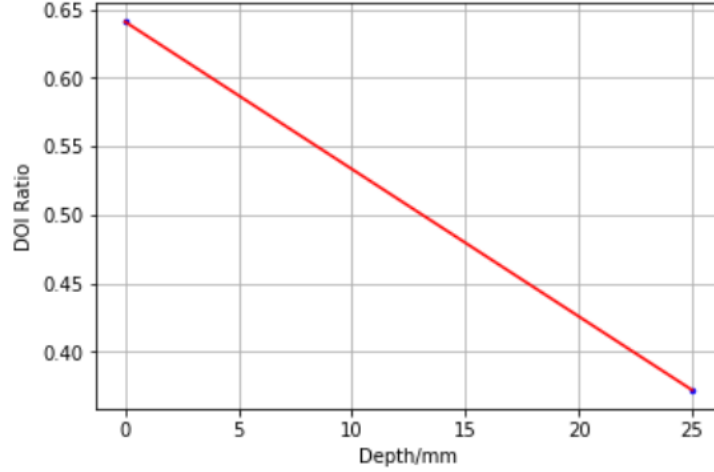
**Figure 8**. DOI responses as a function of depth.



**Figure 9**. Energy spectrum of the scintillator detector with double-ended readout employing a 3 mm × 3 mm × 25 mm unpolished LFS crystal.

Figure 10a and 10b show the relative entrance times of the annihilation photons into the front surface of the crystal as a function of the DOI ratio. The relative entrance times were calculated by subtracting the trigger time of the reference detector from the entrance times of the annihilation photon as calculated from eq. (2.4) and (2.5). Similarly, figure 10c and 10d show the relative trigger times of the photodetectors as function of DOI ratio. The relative trigger times were calculated by subtracting the trigger time of the reference detector from the trigger times of the photodetectors 1 and 2. The results show that the relative times obtained by photodetectors at both ends of the long crystal follows a linear relationship with the DOI. Depending on random interaction points of 511 keV annihilation photons in the crystal, there are depth-dependent residual time variations due to effects such as trigger walk and optical photon time dispersion. These can be used to correct the trigger times of photodetectors 1 and 2. Thus, $t_{relE1}$, $t_{relE2}$, $t_{rel1}$, $t_{rel2}$ were obtained fitting the data with linear relationships to correct the entrance times of the annihilation photons and trigger times of individual photodetectors 1 and 2.
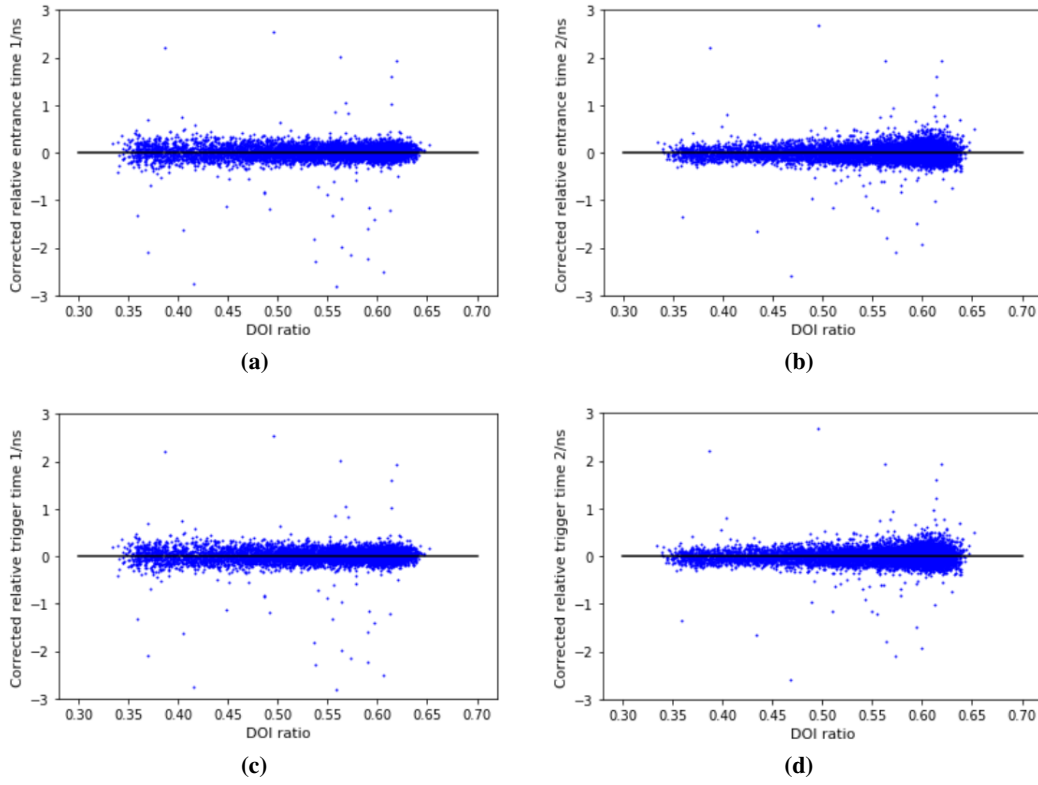
Figure 11a–11d show the corrected relative times as function of DOI ratio after applying the corresponding correction factors ($t_{relE1}$, $t_{relE2}$, $t_{rel1}$, $t_{rel2}$). As the expected, the corrected relative

times now exhibits no observed correlation with DOI. It shows that the two depth-dependent timing-correction methods can achieve same correction results. The variances of the corrected relative trigger times are obtained by histogramming the relative corrected times in multiple bands of the DOI and then fitting the distribution with a Gaussian. Then the variances of the corrected trigger times are calculated by subtracting the variance of the reference detector, which is the square of the standard deviation of the measured timing resolution of the reference detector, from the variances of the corrected relative trigger times. Figure 12a and 12b show the normalized inverse variance weighting factors as a function of the DOI ratio for the corrected entrance times and corrected photodetector trigger times respectively, which were used to calculate the weighted average of the trigger time of the test detector. The results show that the normalized inverse variance weighting factors are independent whether the corrected entrance times or the corrected trigger times we use.
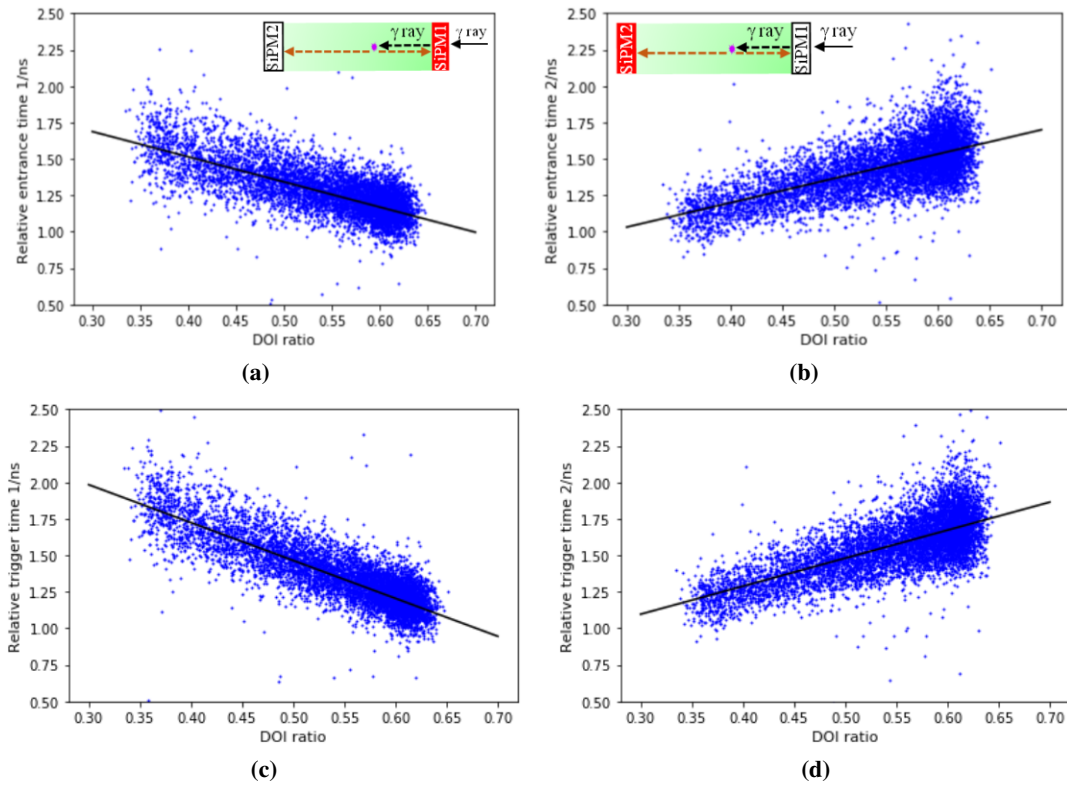


**Figure 10**. Relative times of scintillator detector with double-ended readout against the trigger time of reference detector as a function of the DOI ratio. (a) Relative entrance times of the annihilation photons for photodetector 1. (b) Relative entrance times of the annihilation photons for photodetector 2. (c) Relative trigger times of the photodetector 1. (d) Relative trigger times of the photodetector 2.

Table 2 summarizes the measured CTRs and corresponding calculated CTRs for pairs of the detectors obtained by the different methods described in section 2.2. Using the entrance times in method 2, which corrects the depth-dependent annihilation photon transit time, the CTRs were slightly better than just using the trigger times in method 1. By further correcting for the correlation between the relative times and DOI, the CTRs using depth-dependent timing-correction and weighted average time method in method 3 and 4 were better than in method 2. Table 3 summarizes the corrections of the applied methods.

**Figure 11**. Corrected relative times of scintillator detector with double-ended readout against the trigger time of reference detector as a function of the DOI. (a) Corrected relative entrance times of the annihilation photons for photodetector 1. (b) Corrected relative entrance times of the annihilation photons for photodetector 2. (c) Corrected relative trigger times of the photodetector 1. (d) Corrected relative trigger times of the photodetector 2.
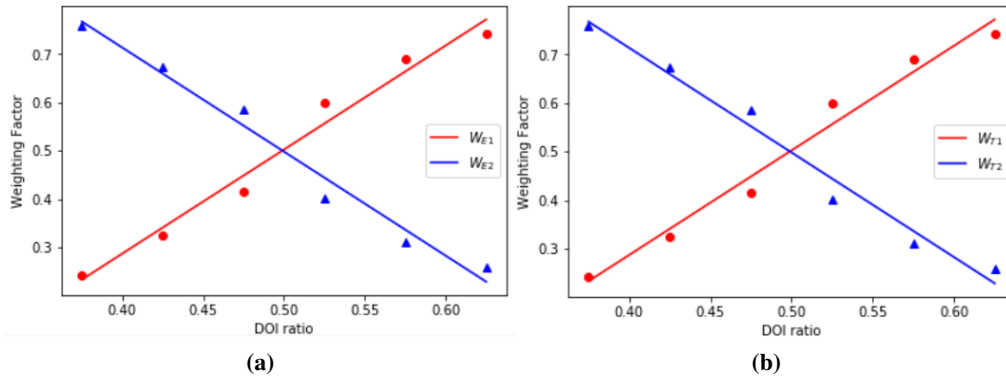


**Figure 12**. Normailzed inverse weighting factors as a function of DOI ratio for (a) the corrected entrance times for photodetector 1 and 2; and (b) the corrected photodetector 1 and 2 trigger times.

The results show that the measured CTR from double-ended readout for polished crystals (238 ps) performs similarly to single-ended readout (235 ps). Figure 7 shows that the DOI ratio for polished crystals is narrowly centered around 0.5, which indicates that the total number of detected

photons are equally divided between the two photodetectors at both ends. This may suggest that the earliest detected optical photons dominantly affect the timing performance of the detector in a polished crystal. The earliest detected optical photons undergo specular reflection are combined in double-ended readout in a similar way as if they are detected by a single photodetector in single-ended readout.

One observation is that taking the simple average of the photodetector trigger times in method 1 perform slightly worse than taking the simple average of the entrance times in method 2. It can be seen in eq. (2.4) and (2.5) that a variation of $\Delta Z$ in the DOI causes the trigger times of photodetector 1 to vary as $\Delta Z/c + n\Delta Z/c$ and the trigger times of photodetector 2 to vary as $\Delta Z/c - n\Delta Z/c$. Thus, the simple average in method 1 cause the trigger times to vary as $\Delta Z/c$, and its timing precision is limited by the variations in the annihilation photon interaction depth [17].

Another observation is that the weighted average performs better than the simple average, which confirms that the simple average is not the best statistical estimator to combine the trigger times of the two photodetectors from a double-ended readout detector [17]. In addition, the correlation between the entrance times and the DOI in figure 10a and 10b suggests that additional depth-dependent effects still remain such as the variation in the trigger delay from the arrival of the first possible photon at the photodetector. By correcting for this remaining depth-dependent effects in method 3 improves the CTR.

Alternatively, all depth-dependent effects can be effectively corrected by just looking at the correlation between the trigger times of the photodetectors and the DOI in figure 10c and 10d in method 4. As expected, the CTRs obtained from method 4 are similar to method 3.

In order to measure DOI, unpolished crystals have to be utilized. However, figure 5 shows that the CTRs from unpolished crystals has worse timing performance than polished crystals. By correcting for all depth-dependent effects in double-ended readout, we improve the CTRs of unpolished crystals by about 37% over single-ended readout. If some light absorption can be introduced in polished crystals to produce different number of detected photons at both ends of the crystal as a function of the interaction depth without degrading the timing resolution, our studies suggest that the timing resolution of detectors utilizing long scintillation crystals with double-ended readout can approach the timing resolution achieved with short polished crystals.

## 4  Conclusion

In this work, the improvement in the timing resolution of TOF-PET detector using double-ended readout were investigated. In order to measure DOI, the crystal surface has to be roughened, which degrades the CTR compared to a polished crystal. A number of methods to calculate the CTRs of double-ended readout detector were studied. The results show that the CTR of double-ended readout based on unpolished crystal is significantly better than single-ended readout. The double-ended readout corrects for almost all of the depth-dependent effect in the detector. Using weighted factors that correspond to the inverse variances of the two photodetectors corrected trigger times give better CTRs than the simple average time method. For $3\,\mathrm{mm} \times 3\,\mathrm{mm} \times 25\,\mathrm{mm}$ unpolished LFS crystal, we obtained a CTR of 246 ps FWHM using double-ended readout compared to 393 ps FWHM using single-ended readout, which corresponds to a 37% improvement. Double-ended readout is an effective method to correct for almost all of the depth-dependent effect in TOF-PET

**Table 2**. Measured CTRs and corresponding calculated CTRs for pairs of the test detectors. S and W represent simple and weighted average respectively.

| Measured Crystal: 3 mm × 3 mm × 25 mm | | Measured CTR | Calculated CTR |
|---|---|---|---|
| Polished | S | 238 ps | 280 ps |
| Unpolished | Individual photodetector 1 | 347 ps | 453 ps |
| | Individual photodetector 2 | 430 ps | 579 ps |
| | Method 1　　　　S | 238 ps | 280 ps |
| | Method 2　　　　S | 231 ps | 267 ps |
| | Method 3　　　　S | 230 ps | 267 ps |
| | Method 3　　　　W | 219 ps | 246 ps |
| | Method 4　　　　S | 230 ps | 267 ps |
| | Method 4　　　　W | 219 ps | 246 ps |

**Table 3**. Corrections of the applied methods (Y=Yes, N=No).

| Method | Single ended | 1 | 2 | 3S,4S | 3W,4W |
|---|---|---|---|---|---|
| Estimate of DOI | N | N | Y | Y | Y |
| Annihilation photon time spread | N | N | Y | Y | Y |
| Direct optical photon time spread | N | Y | N | Y | Y |
| Trigger walk vs. DOI spread | N | N | N | Y | Y |
| Statistically weighted averages | N | N | N | N | Y |

detectors resulting in performance improvement in the timing resolution especially in unpolished long crystals. In addition, double-ended readout enables DOI, which corrects for the parallax errors in PET system to improve the spatial resolution. However, double-end readout detectors would increase the cost and complexity of the overall system.

## Acknowledgments

## A  Variables and abbreviations

Table 4 lists variables used in the calculations.

**Table 4.** Glossary of variables used in the calculations.

| | |
|---|---|
| $CTR_{meas}$ | Measured coincidence timing resolution for single-ended readout (SiPM2) of a scintillator of length L and a 3 mm reference scintillator |
| $CTR_{ref}$ | Coincidence timing resolution between two 3 mm reference scintillators |
| $CTR_{cal}$ | Calculated coincidence timing resolution between two scintillators of length L (eq. (2.1)). |
| $T_{SiPM1}$ | Trigger time of front SiPM1 |
| $T_{SiPM2}$ | Trigger time of rear SiPM2 |
| $T_S$ | Simple average of SiPM trigger times (Method 1) |
| $L$ | Crystal length in direction of annihilation photon |
| $Z$ | Depth of interaction estimated from SiPM pulse height ratio |
| $n$ | Refractive index of scintillation crystal |
| $E_{SiPM1}$ | Annihilation photon entrance time estimated from SiPM1 trigger time plus annihilation and direct optical photon transit times (Method 2, eq. (2.4)) |
| $E_{SiPM2}$ | Annihilation photon entrance time estimated from SiPM2 trigger time plus annihilation and direct optical photon transit times (Method 2, eq. (2.5)) |
| $T_{SE}$ | Simple average of $E_{SiPM1}$ and $E_{SiPM2}$ (Method 2, eq. (2.6)) |
| $t_{relE1}$ | Depth-dependent trigger delay correction factor for $E_{SiPM1}$ |
| $t_{relE2}$ | Depth-dependent trigger delay correction factor for $E_{SiPM2}$ |
| $T_{SEC}$ | Simple average of the corrected entrance times (Method 3S, eq. (2.7)) |
| $W_{E1}$ | 1/Variance of corrected entrance time 1 from calibration |
| $W_{E2}$ | 1/Variance of corrected entrance time 2 from calibration |
| $T_{WEC}$ | Inverse variance weighted average of the corrected entrance times (Method 3W, eq. (2.8)) |
| $t_{rel1}$ | Depth-dependent trigger delay correction factor for $T_{SiPM1}$ |
| $t_{rel2}$ | Depth-dependent trigger delay correction factor for $T_{SiPM2}$ |
| $T_{SC}$ | Simple average of the corrected trigger times (Method 4S, eq. (2.9)) |
| $W_{T1}$ | 1/Variance of corrected photodetector trigger time 1 from calibration |
| $W_{T2}$ | 1/Variance of corrected photodetector trigger time 2 from calibration |
| $T_{WC}$ | Inverse variance weighted average of the corrected photodetector trigger time (Method 4W, eq. (2.10)) |

# References

[1] J.S. Karp, S. Surti, M.E. Daube-Witherspoon and G. Muehllehner, *Benefit of time-of-flight in PET: Experimental and clinical results*, *J. Nucl. Med.* **49** (2008) 462.

[2] M. Conti, *Focus on time-of-flight PET: the benefits of improved time resolution*, *Eur. J. Nucl. Med. Mol. Imaging* **38** (2011) 1147.

[3] S. Gundacker, A. Knapitsch, E. Auffray, P. Jarron, T. Meyer and P. Lecoq, *Time resolution deterioration with increasing crystal length in a TOF-PET system*, *Nucl. Instrum. Meth.* **A 737** (2014) 92.

[4] S. Gundacker et al., *Time of flight positron emission tomography towards* $100 \, ps$ *resolution with L(Y)SO: an experimental and theoretical analysis*, 2013 *JINST* **8** P07014.

[5] D.R. Schaart et al., *LaBr$_3$:Ce and SiPMs for time-of-flight PET: achieving* $100 \, ps$ *coincidence resolving time*, *Phys. Med. Biol.* **55** (2010) N179.

[6] M.V. Nemallapudi et al., *Sub-*$100 \, ps$ *coincidence time resolution for positron emission tomography with LSO:Ce codoped with Ca*, *Phys. Med. Biol.* **60** (2015) 4635.

[7] S. Gundacker et al., *State of the art timing in TOF-PET detectors with LuAG, GAGG and L(Y)SO scintillators of various sizes coupled to FBK-SiPMs*, 2016 *JINST* **11** P08008.

[8] E. Berg and S.R. Cherry, *Using convolutional neural networks to estimate time-of-flight from PET detector waveforms*, *Phys. Med. Biol.* **63** (2018) 02LT01.

[9] H.T. van Dam et al., *A practical method for depth of interaction determination in monolithic scintillator PET detectors*, *Phys. Med. Biol.* **56** (2011) 4135.

[10] G. Borghi, V. Tabacchini and D.R. Schaart, *Towards monolithic scintillator based TOF-PET systems: practical methods for detector calibration and operation*, *Phys. Med. Biol.* **61** (2016) 4904.

[11] W. Moses and S. Derenzo, *Design studies for a PET detector module using a PIN photodiode to measure depth of interaction*, *IEEE Trans. Nucl. Sci.* **41** (1994) 1441.

[12] G. Borghi, B.J. Peet, V. Tabacchini and D.R. Schaart, *A* $32 \, mm \times 32 \, mm \times 22 \, mm$ *monolithic LYSO:Ce detector with dual-sided digital photon counter readout for ultrahigh-performance TOF-PET and TOF-PET/MRI*, *Phys. Med. Biol.* **61** (2016) 4929.

[13] Z. Kuang et al., *Development of depth encoding small animal PET detectors using dual-ended readout of pixelated scintillator arrays with SiPMs*, *Med. Phys.* **45** (2017) 613.

[14] S. Ren, Y. Yang and S.R. Cherry, *Effects of reflector and crystal surface on the performance of a depth-encoding PET detector with dual-ended readout*, *Med. Phys.* **41** (2014) 072503.

[15] S. Seifert and D.R. Schaart, *Improving the time resolution of TOF-PET detectors by double-sided readout*, *IEEE Trans. Nucl. Sci.* **62** (2015) 3.

[16] H.G. Kang, G.B. Ko, J.T. Rhee, K.M. Kim, J.S. Lee and S.J. Hong, *A dual-ended readout detector using a meantime method for SiPM TOF-DOI PET*, *IEEE Trans. Nucl. Sci.* **62** (2015) 1935.

[17] S.E. Derenzo, W.-S. Choong and W.W. Moses, *Monte Carlo calculations of PET coincidence timing: single and double-ended readout*, *Phys. Med. Biol.* **60** (2015) 7309.

[18] S. Ritt, R. Dinapoli and U. Hartmann, *Application of the DRS chip for fast waveform digitizing*, *Nucl. Instrum. Meth.* **A 623** (2010) 486.

[19] Y. Yang et al., *Depth of interaction resolution measurements for a high resolution PET detector using position sensitive avalanche photodiodes*, *Phys. Med. Biol.* **51** (2006) 2131.

[20] Y. Yang et al., *Depth of interaction calibration for PET detectors with dual-ended readout by PSAPDs*, *Phys. Med. Biol.* **54** (2008) 433.